CrystEngComm

Accepted Manuscript

This article can be cited before page numbers have been issued, to do this please use: J. pisk, T. Hrenar, M. Rubi, G. Pavlovi, V. Damjanovi, J. Lovri, M. Cindri and V. Vrdoljak, *CrystEngComm*, 2018, DOI: 10.1039/C7CE02136D.

ROYAL SOCIETY OF CHEMISTRY

rsc.li/crystengcomm

CrystEngComm
CREATED USING THE RSC ARTICLE TEMPLATE (VER. 3.1) - SEE WWW.RSC.ORG/ELECTRONICFILES FOR DETAILS
View Article Online
ARTICLE TYPE www.rsc.org/xxxxxx | XXXXXXXX DOI: 10.1039/XXXXXXXX

Comparative studies on conventional and solvent-free synthesis toward hydrazones: Application of PXRD and chemometric data analysis in mechanochemical reaction monitoring

Jana Pisk,[a] Tomica Hrenar,[a] Mirta Rubčić,[a] Gordana Pavlović,[b] Vladimir Damjanović,[c] Jasna Lovrić,[c] Marina Cindrić,[a] Višnja Vrdoljak*[a]

Received (in XXX, XXX) Xth XXXXXXXXX 200X, Accepted Xth XXXXXXXXX 200X
First published on the web Xth XXXXXXXXX 200X
DOI: 10.1039/b000000x

Synthesis of hydrazones was performed *via* both conventional and solvent-free routes using the corresponding hydrazide (isonicotinic hydrazide, nicotinic hydrazide, 2-aminobenzhydrazide or 4-aminobenzhydrazide) and appropriate aldehyde (salicylaldehyde , 3-methoxysalicylaldehyde or 4-methoxysalicylaldehyde). A systematic study dedicated to solvatomorphism or polymorphism screening resulted in formation of twelve novel crystalline forms, and eight of these were characterized *via* the single crystal X-ray diffraction method. In all studied structures, the molecules were assembled into endless supramolecular chains, discrete rings, chains of rings or nets. The mechanochemical synthesis employing liquid-assisted grinding was also applied and the nicotinic- and isonicotinic-based hydrazones were found to form readily from their corresponding precursors. The chemometric study using principal component analysis for mechanochemical synthesis monitoring was implemented for the first time to provide an insight on the reaction profiles. A thoughtful combination of *ex situ* powder X-ray diffraction method and chemometric analysis was essential to identify a stepwise mechanism for the hydrazone formation *via* an intermediate phase. In five investigated reactions the first principal component accounted for at least 75% of the total variance, whereas in the case of two reactions this component accounted for 69.72 and 46.23% of the total variance. The hydrazones were also evaluated for cytotoxic activity *in vitro*. All compounds exhibited weak to moderate cytotoxicity against THP-1 and no cytotoxicity against HepG2 cells. Substantial antibacterial activity was obtained against *Moraxella catarrhalis* while no growth inhibition of *Staphylococcus aureus*, *Enterococcus faecalis* *Escherichia coli* was observed.

Introduction

Short- and long-term environmental issues are one of the most challenging and prominent key points of academy and industry. The necessity of greener conditions has led to development of solventless protocols that impose themselves as the future of sustainable pathways. In this context, mechanochemistry is suggested as a promising alternative to classical solution-based synthesis of a wide range of compounds and as a potential method to obtain novel solid forms.[1–3]

Most of the mechanistic studies of mechanochemical reactions are achieved by *ex situ* identification of the compounds obtained after the reaction. Recently presented methods and techniques have been intended to serve for real time *in situ* reaction monitoring, which provided direct insight into the product formation.[4–8] *In situ* analysis is highly required and needed for the air, moisture or CO_2 sensitive reactions.[9,10]

Lately, mechanochemistry has gained momentum in synthesis of active pharmaceutical ingredients (APIs).[11] It is well known that aroylhydrazones represent an important group of active molecules having numerous biological properties.[12–15] The first synthesis of hydrazones using ball-milling method was reported by Kaupp and coworkers.[16,17] Moreover, Baltas *et al.* recently reported solvent-free route for pharmaceutically attractive phenol hydrazones using a vibratory ball mill.[18]

In continuation to our previous work,[19-21] we aimed to investigate synthesis and properties of a series of aroylhydrazones (Scheme 1). The idea in this work was to test for the first time the implementation of chemometric analysis using principal component analysis (PCA) for the mechanochemical synthesis monitoring.

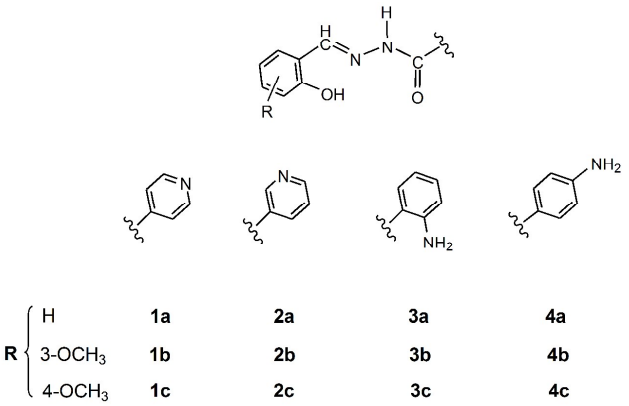

Scheme 1 Structures of aroylhydrazones

View Article Online
DOI: 10.1039/C7CE02136D

This part involved: (1) optimization of the experimental conditions for the solvent-free synthesis; (2) *ex-situ* monitoring of the synthesis by the powder X-ray diffraction method (PXRD); and (3) data evaluation using PCA. We showed how combining analyses based on PXRD technique and chemometric method easily allow identification of an intermediate phase and help in generating reaction profiles.

Pseudopolymorphic or polymorphic form outcome is very important for APIs as they could have different physical and chemical properties.[22–24] Therefore, a systematic study dedicated to solvatomorphism or polymorphism screening was undertaken. Since the occurrence of solvated crystalline forms may not always be of direct significance to a particular product, the products of desolvation were also obtained and characterized.

Analytical tools were applied in order to determine properties of each product (whether it was amorphous or crystalline, a single form or mixed solid phases, a known form or novel form, or it was different solvate). All forms were additionally compared to the ones known from Cambridge Structural Database (CSD).[25–37] We were particularly interested to investigate the influence of the solvent molecules on intermolecular interaction patterns and crystal packing features. In the end, cytotoxic and antibacterial activities of the obtained compounds against selected human cancer cell lines and Gram-positive and Gram-negative bacterial strains were assessed.

Results and Discussion

Solution based synthesis and solid state transformations of the solvated forms

All hydrazones were prepared by the condensation reaction of the corresponding hydrazide (isonicotinic hydrazide (**1**), nicotinic hydrazide (**2**), 2-aminobenzhydrazide (**3**) or 4-aminobenzhydrazide (**4**)) with aromatic aldehyde (salicylaldehyde (**a**), 3-methoxysalicylaldehyde (**b**) or 4-methoxysalicylaldehyde (**c**)), Table 1, Schemes S1 and S2 (see ESI†). In the case of the 2-amino- and 4-aminobenzhydrazide it was important to maintain equimolar amounts of the hydrazide and aldehyde while keeping the reaction temperature below 40 °C. Under these conditions, only one condensation reaction occurred while the amine functional group on phenyl ring remained free.

Investigation of reaction conditions in methanol or ethanol was carried out comprehensively to explore potential formation of different crystalline forms. As a result, new hydrazone forms were achieved and crystal structures of **2b·MeOH, 2c·MeOH**, **3b**, **4a**, **4b·MeOH**, **4b·EtOH** and **4c** were determined by the single crystal X-ray diffraction method. PXRD patterns allowed the comparison of results with literature data as well as with those simulated from the single crystal experiment (Figs. S1−S4, see ESI†). Fast evaporation under vacuum led to the formation of solvent-free forms, whereas longer crystallization processes favoured formation of the solvates either with one methanol (or ethanol) molecule (**2b·MeOH**, **2c·MeOH**, **4b·MeOH** and **4b·EtOH**) or with one water molecule (**1c·H_2O**, **2a·H_2O**, **2b·H_2O**, **2c·H_2O** and **4b·H_2O**). All hydrates were grown from an ethanolic solution exposed to atmospheric moisture.

Crystallization from other organic solvents (Table S1) led to formation of hydrates or unsolvated forms most probably due to the specific intermolecular interactions formed between hydrazones or between hydrazone and water molecules.

Before any attempt to perform the desolvation reactions, thermal stability of the hydrazones was examined (see TG analysis). Compound **4b·MeOH** was the most unstable and we were not able to obtain its experimental PXRD pattern due to its very fast transformation to **4b** (Figs. S4 and S5, see ESI†). Crystals of **2b·MeOH** and **2c·MeOH** tend to lose solvent of crystallization upon grinding (Fig. S2). After prolonged grinding of **2b·MeOH**, **2c·MeOH**, and **4b·EtOH** at room temperature a complete desolvation led to formation of the crystalline forms **2b**, **2c-I** and **4b**, respectively, Scheme 2. These transformations were also followed by the powder X-ray diffraction methods (Fig. S5).

Table 1 Synthesis of hydrazones.

Hydrazone	Solution based method	Mechanochemical synthesis	Desolvation of solvates
1a	+	+	
1b	+	+	
1c	+		+
1c·H_2O	+		
2a-I and 2a-II	+[a]		+
2a·H_2O	+	+	
2b			+
2b·H_2O	+	+	
2b·MeOH	+		
2c-I and 2c-II			+[b]
2c·H_2O	+	+	
2c·MeOH	+		
3a	+		
3b	+	+	
3c	+		
4a	+		
4b	+		+
4b·H_2O	+		
4b·MeOH	+		
4b·EtOH	+		
4c	+		

[a] **2a-I** was obtained by the condensation reaction in MeOH; **2a-II** was obtained upon crystallization from acetone and MeCN; **2c-I** was obtained upon desolvation from **2c·MeOH**; **2c-II** was obtained upon dehydration.

Additionally, a thermally induced desolvation of the hydrates was performed (Scheme 2). The absence of solvent molecule in **1c·H_2O** resulted in formation of **1c** (CSD code KUTPOF) whereas the dehydration of **2c·H_2O** and **4b·H_2O** resulted in the crystalline forms **2c-II** and **4b**, respectively, which could not be obtained directly by the solution based method. In the case of **2a·H_2O** and **2b·H_2O** the resulting diffraction patterns of the unsolvated forms revealed the amorphous nature of the solids (Fig. S6, see ESI†).

View Article Online
DOI: 10.1039/C7CE02136D

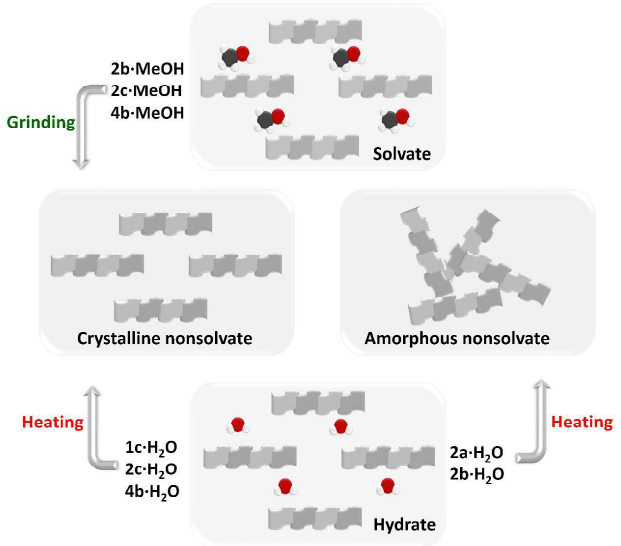

Scheme 2 Graphical scheme of the dehydration/desolvation reactions in the solid state

Mechanochemical synthesis

Initially, mechanochemistry was employed in the synthesis of the isonicotinic- and nicotinic-based hydrazones. The liquid-assisted grinding technique (LAG) in a ball mill of the starting reagents in presence of a small amount of methanol was used in all cases except for the compounds derived from salicylaldehyde, where reagent was used as a liquid. Five hydrazones were successfully obtained in such a way, the unsolvated forms **1a** and **1b** and monohydrates **2a·H_2O**, **2b·H_2O** and **2c·H_2O**. In comparison to the conventional solution based method, the mechanochemical synthesis resulted in the quantitative conversion. The powder X-ray diffraction revealed the complete disappearance of reflections corresponding to starting compounds after 10-60 min if reactions were conducted at 25 Hz. The lack of the starting compounds in the final products was also confirmed by the FT-IR − ATR spectroscopy.

The diffractograms of samples obtained from the 4-methoxysalicylaldehyde and isonicotinic hydrazide indicated a very fast formation of the intermediate (see ESI Scheme S2†) with significantly lower chemical reactivity.[38,39] Afterward, the PXRD patterns revealed the partial disappearance of the X-ray reflections corresponding to the intermediate and concomitant appearance of the diffraction features consistent with those calculated from known crystal structure of **1c·H_2O**. However, formation of the pure product **1c·H_2O** was not achieved even after 270 min milling time (Fig. S7).

The aminobenzhydrazone compounds **3a-3c** and **4a-4c** could not be obtained selectively under the above mentioned conditions due to formation of by-products (imines or quinazolinones). Only in the case of **3b**, when reaction proceeded at 10 Hz, formation of the target hydrazone *via* mono-functionalisation of the 2-aminobenzhydrazide was successfully achieved.

Ex-situ reaction monitoring using powder X-ray diffraction method and chemometrics

One of the main objectives of this work is the application of chemometric tools for PXRD data analysis obtained by reaction monitoring. To test feasibility, it was necessary to develop optimized reaction conditions (frequency, number of milling balls and the addition of small quantities of solvent) that provide a suitable reaction progress for *ex-situ* monitoring and chemometric data analysis.

For this purpose, the best conditions were applied and LAG reactions were conducted using a ball mill operating at a frequency of 25 Hz (**1a** and **2a·H_2O**), 10 Hz (**1b**, **2b·H_2O** and **3b**) and 20 Hz (**2c·H_2O**), and 25 µL of methanol and one milling ball. Performing multiple runs allowed synthesis progress to be followed *ex-situ* as a function of time without disturbing reaction mixture. A sample of the powder obtained after a particular reaction time was immediately analyzed by using the PXRD method (no purification of the powder was performed). Comparison of the patterns of the finally obtained hydrazones and those calculated from the single crystal X-ray crystallography studies (Fig. 1) confirmed the composition of the mechanosyntesized hydrazones. PXRD patterns for *ex-situ* monitoring and chemometric data analysis are given in Figs. 2-5 and Figs. S7-S11. They show a comparison of patterns between the starting materials and reaction progress as a function of time.

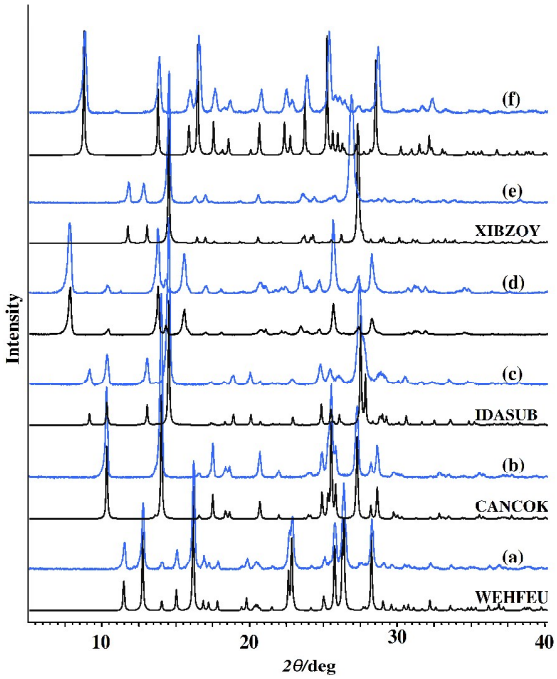

Fig. 1 PXRD patterns of the mechanochemically prepared hydrazones (the blue lines) and simulated patterns (the black lines with refcode) of (a) **1a** (50 min reaction), CSD code WEHFEU;[25] (b) **1b** (70 min reaction), CSD code CANCOK;[29] (c) **2a·H_2O** (90 min reaction), CSD code IDASUB,[35] and (e) **2c·H_2O** (150 min reaction), CSD code XIBZOY[36]; (d) PXRD pattern of the mechanochemically prepared **2b·H_2O** (the blue line, 70 min reaction) and of the sample obtained by the solution based method (the black line); (f) PXRD patterns of the mechanochemically prepared **3b** (90 min reaction) and calculated from the crystal structure **3b** (the black line).

View Article Online
DOI: 10.1039/C7CE02136D

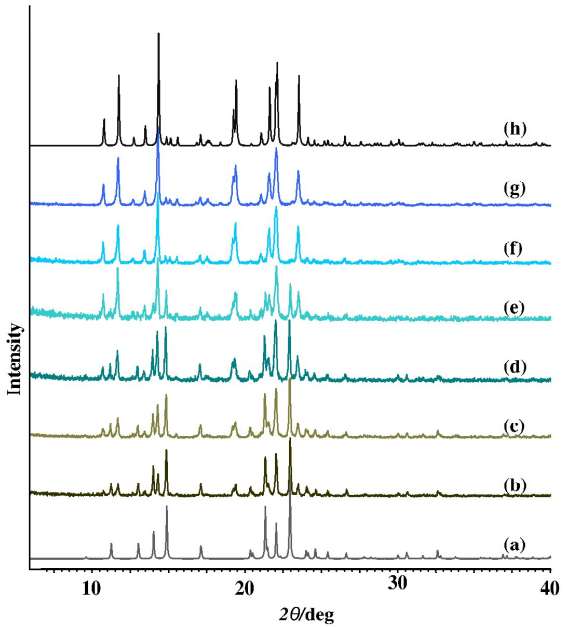

Fig. 2 (a) PXRD patterns of pure isonicotinic hydrazide (refcode: INICAC); *Ex-situ* X-ray diffraction analysis of the 1:1 reaction between salicylaldehyde and isonicotinic hydrazide after (b) 10 min; (c) 20 min; (d) 25 min; (e) 30 min; (f) 40 min; (g) 50 min; and (h) PXRD patterns of **1a** calculated from the deposited crystal structure (refcode: WEHFEU).

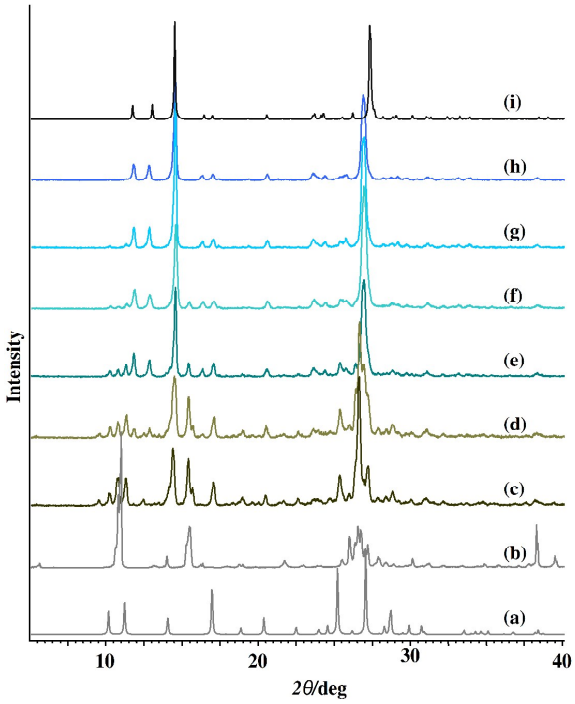

Fig. 3 (a) PXRD patterns of pure nicotinic hydrazide calculated from the deposited crystal structure (refcode: GIRYEM); (b) PXRD patterns of pure 4-methoxysalicylaldehyde; *Ex*-situ X-ray diffraction analysis at room temperature of the 1:1 reaction between 4-methoxysalicylaldehyde and nicotinic hydrazide after (c) 30 min; (d) 50 min; (e) 70 min; (f) 90 min; (g) 120 min; (h) 150 min and (i) PXRD patterns of **2c·H$_2$O** calculated from the deposited crystal structure (refcode: XIBZOY; X-ray study at 150K).

Table 2 Total variance represented by the first 6 principal components calculated for a set of PXRD data collected through mechanochemical syntheses

Component	**1a**	Cumulative	**1b**	Cumulative	**3b**	Cumulative
PC1	82.87	82.87	69.72	69.72	46.23	46.23
PC2	8.15	91.02	25.34	95.06	37.90	84.13
PC3	4.50	95.52	3.60	98.66	11.23	95.36
PC4	2.10	97.62	0.76	99.42	2.97	98.33
PC5	0.92	98.54	0.56	99.98	1.67	100.00
PC6	0.84	99.38	0.00	99.98	0.00	100.00
	2a	Cumulative	**2b**	Cumulative	**2c**	Cumulative
PC1	89.91	89.91	89.03	89.03	89.49	89.49
PC2	6.19	96.10	4.83	93.86	8.08	97.57
PC3	3.34	99.44	2.47	96.33	1.33	98.9
PC4	0.28	99.72	2.29	98.62	0.76	99.66
PC5	0.18	99.9	1.35	99.97	0.31	99.97
PC6	0.08	99.98	0.00	99.97	0.00	99.97
	1c	Cumulative				
PC1	74.88	74.88				
PC2	15.88	90.76				
PC3	5.46	96.22				
PC4	3.10	99.32				
PC5	0.68	100.00				
PC6	0.00	100.00				

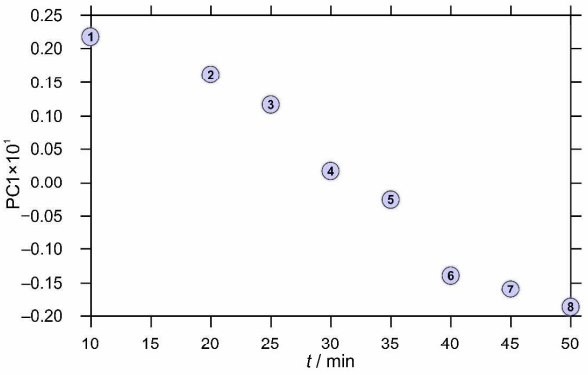

Fig. 4 Time dependence of PC1 scores calculated for a set of PXRD data collected through mechanochemical synthesis of **1a**.

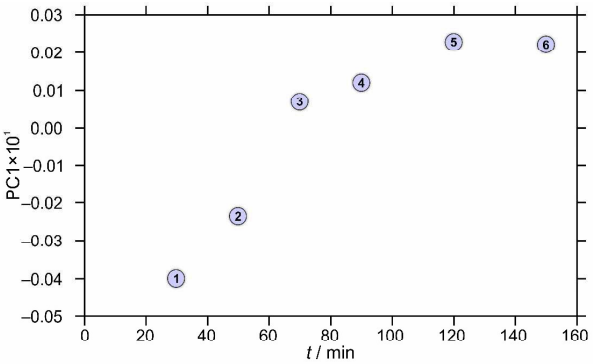

Fig. 5 Time dependence of PC1 scores calculated for a set of PXRD data collected through mechanochemical synthesis of **2c·H$_2$O**.

View Article Online
DOI: 10.1039/C7CE02136D

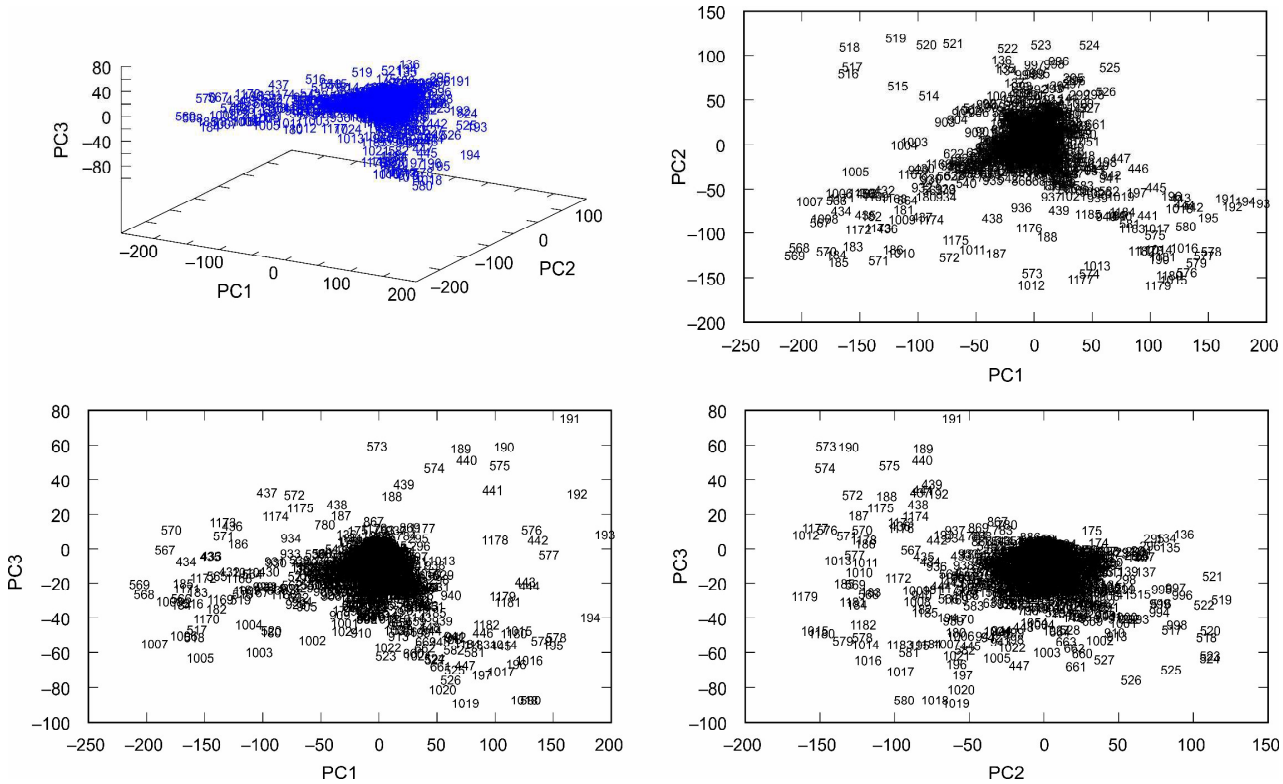

Fig. 6 Principal component loadings calculated for a set of PXRD data collected through mechanochemical synthesis of **3b**.

In general, salicylaldehyde and 4-methoxysalicylaldehyde are less reactive than the 3-methoxy-substituted aldehyde. Comparison of the data for **2b·H$_2$O** implies that the reaction does not proceed any further beyond 10 min of grinding. In the case of **1b** the reaction is almost complete within the first 20 min and after that time only a small additional amount of product is formed.

According to the analysis of the PXRD patterns (Table 2, Figs. 4 and 5), the reaction profiles can be well represented using only the 1st principal component. In each case where the PC1 describes more than 70% of the total variance, this reaction profile nicely shows the progress and the end of the reaction. Investigation of PXRD patterns confirmed that reactions were completed in the time predicted by the PC1 reaction profiles.

In the case of **1b** and **3b** formation of a reaction intermediate was noticed. Total variance described in the first principal component was less than 70%. For the formation of **1b** and **3b**, it was 69.72 and 46.23% respectively. These lower values of the total variance indicate some other types of reactions in the investigated systems. More probably, the two or even more consecutive reactions were present and the formation of the reaction intermediate occurred.

Principal component loadings in 3-dimensional space show a particular symmetrical "butterfly" pattern (Fig. 6). This symmetrical pattern along with the principal components indicates the almost equal importance of the orthogonal eigenvectors extracted from the original PXRD data. Since first 2 principal components explain nearly equal amounts of variance, it is reasonable to expect that two or even more reactions are occurring simultaneously.

Molecular structures of 2b·MeOH, 2c·MeOH, 3b, 4a, 4b·MeOH, 4b·EtOH, 4b·H$_2$O and 4c

The general crystallographic data along with the final data collection parameters and refinement statistics, selected bond distances and torsion angles, dihedral angles and hydrogen bonds geometry are given in Tables 3, S1-S4, see ESI†), respectively. The asymmetric units of **3b**, **4b·MeOH**, **4b·EtOH** and **4c** contain two crystallographically independent molecules.

The solid-state structures (Fig. 7, Figs. S12-S14, see ESI†) reveal that all molecules are in the amide tautomeric form with *E* configuration. The –NH and C=O groups of the amide fragment exhibit *trans* spatial orientation, as it is expected due to spatial demands of substituents leading to van der Waals repulsion minimization. This can be described also as *synperiplanar* conformation considering restricted rotation around the amide C–N single bond (see the torsion angle N2–N1–C1–C2 values in Table S2 denoted as τ).

The values of torsion angles τ and φ, first describing the *N*-aroyl substituent rotation and another, describing blocked rotation around C8–C7 and C8–C9 bonds, predominantly σ in character, in nicotinic hydrazide derivatives and aminobenzhydrazide derivatives, respectively (Table S2) are endorsement of the planarity of the central molecular moiety =N−NH−(C=O)−. The rotation around these bonds (C8–C7 or C8–C9) is blocked due to the existence of O–H···N intramolecular hydrogen bond between the hydroxyl group and the imino nitrogen atom N2 forming six-membered pseudoaromatic ring described by the graph-set notation as *S*(6) in all structures.

View Article Online
DOI: 10.1039/C7CE02136D

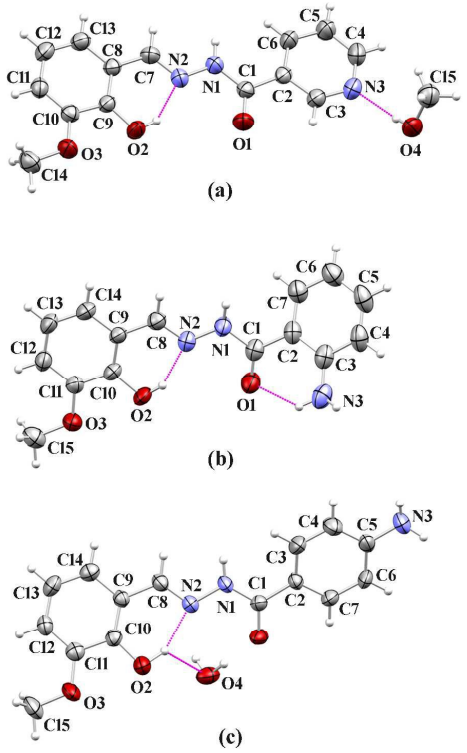

Fig. 7 Mercury-POV-Ray drawing of the asymmetric units of selected molecular structures of hydrazones: (a) **2b·MeOH**; (b) **3b** and (c) **4b·H$_2$O**. The displacement ellipsoids are drawn at the 50 % probability level at 296(2) K. The hydrogen atoms are drawn as spheres of arbitrary radius. Intramolecular hydrogen bonds within asymmetric unit are shown as pink dashed lines.

The bond distances of =N−NH−(C=O)− moiety *i.e.* correlate with above considerations (ESI Table S2). On the contrary to the planarity of the central molecular fragment, the molecules are not planar as a whole which is confirmed by the dihedral angles between phenyl rings planes (ESI Table S3). The planarity is more pronounced in nicotinic hydrazide derivatives than in aminobenzohydrazide derivatives amounting 2.2(1) and 6.1(1)° in **2c·MeOH** and **2b·MeOH** structures, respectively, while in aminobenzhydrazide derivatives the dihedral angles between phenyl rings planes are in the range 19.1(1) - 37.0(2)° (Fig. 8). There is no correlation between the presence of the solvent of crystallization and molecular planarity due to the possible more complex hydrogen bonds network with the crystallization solvents.

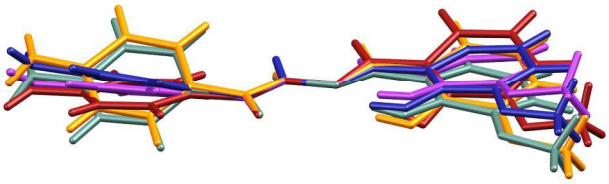

Fig. 8 Mercury-POV-Ray rendered view of overlapping diagram for 4-aminobenzhydrazide-based hydrazones (**4b·H$_2$O** – red, **4b·MeOH** – two crystallographically independent molecules in dark yellow and green, **4b·EtOH** – two crystallographically independent molecules in magenta and blue). Diagram was constructed by overlapping molecules through nitrogen and oxygen atoms of central molecular =N−NH−(C=O)− moiety.

Supramolecular architectures of the eight hydrazones and role of solvents of crystallization in the supramolecular assembly

The solid-state structures of eight hydrazones reveal proton donor/acceptor competition of functional groups in supramolecular assembly (for detailed description of supramolecular architecture for each compound see ESI†). It has been found that in all studied structures, molecules form endless supramolecular chains, discrete rings, chains of rings or nets defined by hydrogen bonds.

The frequent supramolecular feature is the appearance of bifurcation which implicates formation of fused hydrogen bonded rings or infinite chains of rings as preferable supramolecular synthons rather than 1D infinite chains. The bifurcation of atoms of solvent molecules is found for the O4 oxygen atom from solvent molecules of crystallization in the structures of **2b·MeOH** (Fig. 9) and **2c·MeOH** (Fig. S15). In the crystal structures of nicotinic hydrazide derivatives **2b·MeOH**, **2c·MeOH** the strong proton acceptor such as pyridine nitrogen atom forms hydrogen bonds exclusively with alcohols.

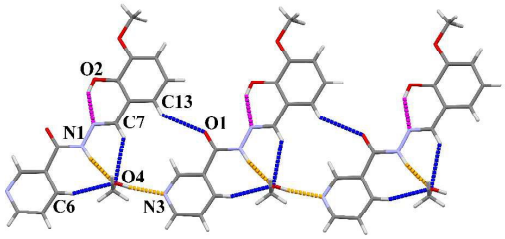

Fig. 9 Supramolecular assembly in compound **2b·MeOH**. Intramolecular hydrogen bond O2···N2 is shown as magenta dashed lines, intermolecular hydrogen bonds of the O–H···N and N–H···O type as dark orange dashed lines, and the weak C–H···O intermolecular hydrogen bonds as blue dashed lines. The same colour scheme for hydrogen bonds has been applied in all crystal structures. Atom-labelling has been applied for non-hydrogen contact atoms within the unit cell.

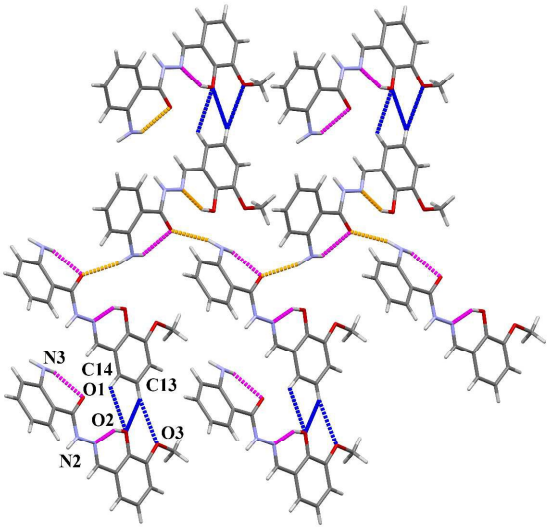

Fig. 10 Supramolecular assembly in compound **3b**. Infinite chains along *a* axis is formed based on two hydrogen bonds: intra N3-H13N···O1 and inter N3–H23N···O1. The chains are stacked along *b* axis.

View Article Online
DOI: 10.1039/C7CE02136D

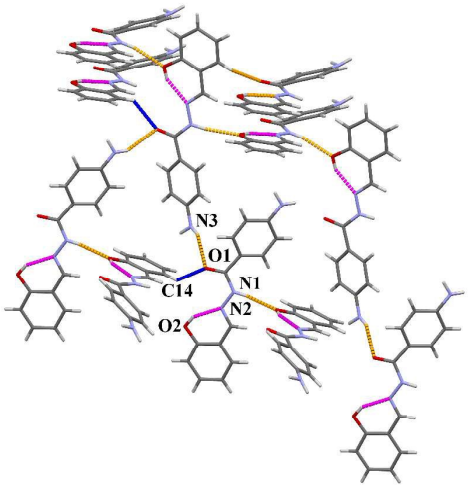

Fig. 11 Supramolecular assembly in compound **4a** into 3D hydrogen bonded network.

Carbonyl oxygen atom O1 in **3b**, **4a** and **2c·MeOH** (Figs. 10, 11 and S24, respectively), hydroxyl O2 atom in **3b** and C13 aryl group in **3b** (Fig. 10) and –NH amine hydrogen atom in **4b·EtOH** and **4b·MeOH** (Figs. 12 and S16, respectively) exhibit bifurcation, too.

The supramolecular function of solvents of crystallization is interlinking hydrazone molecules *via* hydrogen bonds with the carbonyl O1 atom, hydroxyl O2 atom and amine –NH group (Fig. S17). This function in supramolecular architecture is significant since water or alcohols molecules exhibit multiple roles as proton donors and acceptors at the same time. The role of water molecule as the solvent of crystallization is different in comparison with the supramolecular role of methanol and ethanol molecules in **4b·MeOH** (Fig. S16) and **4b·EtOH** (Fig. 12). While the structures of **4b·MeOH** and **4b·EtOH** are similar at the level of strong or moderate hydrogen bonds, the O4 oxygen atom of monohydrate **4b·H_2O** (Fig. 13) possesses multiple roles in hydrogen bond formation interlinking molecules *via* hydrogen bonds with the carbonyl amide O1 atom, hydroxyl O2 atom and amine –NH group (see ESI for detailed description). Further, the simultaneous acting as proton acceptor and donor, results in formation of infinite chains, which is particularly perceived for hydroxyl oxygen atom (**2c·MeOH**, **3b**, **4a**, **4b·EtOH** and **4b·MeOH**).

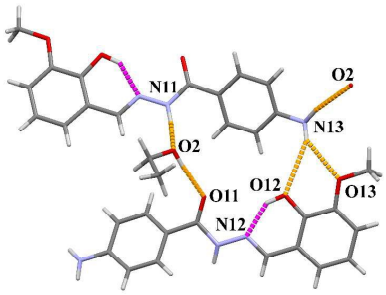

Fig. 12 Supramolecular assembly in compound **4b·EtOH** showing assembling of crystallographically dependent molecules *via* hydrogen bonds into sheets.

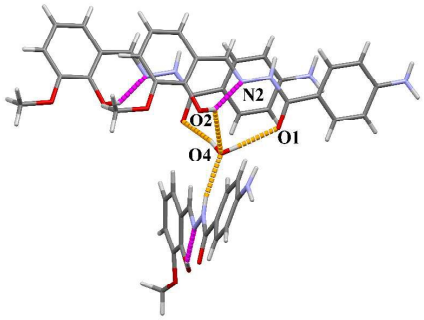

Fig. 13 Supramolecular assembly in compound **4b·H_2O** showing water molecule multiple role in hydrogen bond formation.

A well-known amide group supramolecular pattern of *C*(4) infinite chains between carbonyl amide and –NH amide group defines only **4c** supramolecular structure (Fig. 14).

The crystal structures of compounds without crystallization solvents are dominated with hydrogen bonds including carbonyl amide O1 atom as proton acceptor with amine rather than amide group. Methoxy group participates in the formation of weak hydrogen bonds usually of the C–H···O type, with amine group (only in **4b·MeOH**, **4b·EtOH**) or does not participate at all (**4c**).

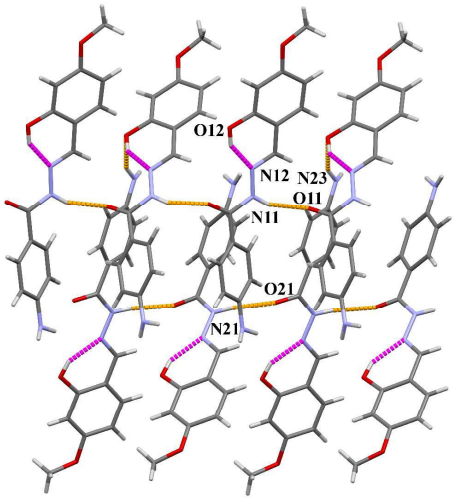

Fig. 14 Supramolecular assembly in compound **4c** showing *C*(4) supramolecular synthon formed between amide nitrogen atoms and carbonyl oxygen atoms.

Spectroscopic characterization

The characteristic IR bands, NMR and UV data are given in ESI. The IR spectra of the hydrazones confirmed the presence of the carbonyl group of the amide tautomer (Scheme S3, see ESI†). This is indicated by the intense absorption in the range of 1690-1620 cm^{-1}. All compounds exhibited a vibration band at *ca*. 1610 cm^{-1} belonging to $C{=}N_{imine}$ group along with an absorption band at *ca*. 2840 cm^{-1} attributed to C−H stretching of the −(C=O)−NH−N=CH− moiety. Additionally, the medium intensity band observed at *ca*. 1150 cm^{-1} is assigned to N−N stretching vibrations. Finally, the spectra of all hydrates showed the absorption band at ~3550 cm^{-1} assigned as O−H stretching which revealed the presence of the crystalline water molecule.

View Article Online
DOI: 10.1039/C7CE02136D

Proton and carbon chemical shifts of all hydrazones (Tables S5-S8, Schemes S4-S7, see ESI†) are assigned by using one (^{1}H and APT) and two-dimensional NMR experiments in DMSO-d_6 (COSY, HMQC and HMBC). The phenyl and py moieties gave signals in the range 9.09-6.50 ppm. Singlets at 8.70-8.48 ppm, 11.88-10.69 ppm and 12.29-11.62 ppm are assigned to azomethyne H, OH and N=NH, respectively. The presence of NH proton signal in all spectra indicates that neither of the compounds is in the iminol tautomeric form =N−N=(C−OH)− but in an amide form =N−NH−(C=O)− (Scheme S3). Singlets at ~6.5 and ~5.8 confirmed the existence of $-NH_2$ in the spectra of compounds **3a-3c** and **4a-4c**, respectively. Additionally, the signals of OH, N=NH and NH_2 protons are somewhat broadened indicating their involvement in hydrogen bonding interactions. ^{1}H NMR spectra of **1b-4b** and **1c-4c** present a singlet at 3.83-3.78 ppm due to the OCH_3 group.

In the ^{13}C NMR spectra **1a-1c** and **2a-2c**, the carbon signals of the pyridine ring due to nitrogen atom are observed at 152.9-122.0 ppm, whereas the carbon signals of the phenyl ring substituted with amino group are found at 150.8-113.0 ppm. Signals appeared in the low field within the range 165.48-161.52 ppm and 150.01-147.32 ppm are attributed to C4 of the carbonyl amide group and C1 carbon of the CH=N group, respectively.

The ^{1}H NMR spectra of isonicotinic- and nicotinic-based hydrazones **1a-1c** and **2a-2c**, respectively, showed two sets of signals with a ratio of intensities *ca*. 1:0.06 (**1a**), 1:0.06 (**1b**) and 1:0.04 (**1c**), 1:0.06 (**2a**), 1:0.07 (**2b**) and 1:0.04 (**2c**). This result indicated presence of the *E*/*Z* imine isomers in the solution at 298 K. In the low integrating set of signals there is an upfield shift of the resonances OH, NH and H-C11 with respect to the high integrating set.

The UV-Vis spectral data of some investigated hydrazones, in different solvents, have been reported in the literature.[40,35] In the UV-Vis spectra of isonicotinic- and nicotinic-based hydrazones appearance of the characteristic bands is very similar for the each aldehyde used. The bands in the range 215-223 nm and 291-333 nm could be assigned to the π-$\pi*$ transition of the aromatic rings and intraligand $n\rightarrow\pi*$ transition, respectively.[41] In the case of salicylaldehyde derivative, additional band at 329 (**1a**) and 335 nm (**2a**) that could be correlated to the charge transfer within the entire Schiff base molecule. This band is usually due to strong intramolecular hydrogen bonding between the hydroxyl group of the salicylidene and the azomethine nitrogen.[42] In the case of hydrazones obtained from aminohydrazidess, bands do not follow exact similarity pattern as those obtained from previously mentioned ones. The first band typical for π-$\pi*$ transition of the aromatic rings, for hydrazone derived from 2-aminobenzhydrazide (**3a-3c**) appeared in 218-223 nm region, while for **4a** and **4b** at 228 and 222 nm, respectively. The second band for **3a-3c** appeared in the region 288-331 nm, while for the hydrazones **4a** and **4b** at 333 and 321 nm, respectively. The third band around 345 nm could be seen in the case of hydrazones **3a-3c**, but not in the case **4a** and **4b**. Hydrazone **4c** has only one characteristic band at 336 nm.

Thermal analysis

The first mass loss in the TG curves of ligands **1c·H$_2$O** and **2a·H$_2$O**, **2b·H$_2$O**, **2c·H$_2$O, 4a·H$_2$O** is related to the water molecule release (6.0%, 6.8%, 5.7% and 6.1%, 5.8%, respectively). The melting endothermic peaks of the anhydrous hydrazones **1c**, **2a** and **2c** are sharp, in narrow temperature interval, directly implying sample purity. From DSC measurements, the melting point for unhydrous form **1c** was at 229 °C ($\Delta_{fus}H$ = 130 kJ mol^{-1}), **2a** at 184 °C ($\Delta_{fus}H$ = 25 kJ mol^{-1}), **2c** at 143 °C ($\Delta_{fus}H$ = 32 kJ mol^{-1}). For **2b** and **4a** it is not possible to distinguish the desolvation and melting processes.

The solvent molecules of the alcohol solvate forms **2b·MeOH**, **2c·MeOH**, **4b·MeOH** and **4b·EtOH** escape easily at room temperature. From DSC measurements, the melting point for unsolvated forms **2b** was at 160 °C ($\Delta_{fus}H$ = 21 kJ mol^{-1}), **2c-I** was at 168 °C ($\Delta_{fus}H$ = 24 kJ mol^{-1}) and **4b** at 228 °C ($\Delta_{fus}H$ = 37 kJ mol^{-1}).

The unsolvated forms crystallized directly from solution have meting onsets found for **1a** at 250 °C ($\Delta_{fus}H$ = 40 kJ mol^{-1}), **1b** at 235 °C ($\Delta_{fus}H$ = 29 kJ mol^{-1}), **1c** was at 229 °C ($\Delta_{fus}H$ = 130 kJ mol^{-1}), **2a** at 190 °C ($\Delta_{fus}H$ = 27 kJ mol^{-1}), **2a-II** at 185 °C ($\Delta_{fus}H$ = 22 kJ mol^{-1}), **3a** was 166 °C ($\Delta_{fus}H$ = 26 kJ mol^{-1}), **3b** at 185 °C ($\Delta_{fus}H$ = 27 kJ mol^{-1}), **3c** at 157 °C ($\Delta_{fus}H$ = 27 kJ mol^{-1}) and **4c** at 225 °C ($\Delta_{fus}H$ = 30 kJ mol^{-1}).

***In vitro* cytotoxic and antibacterial activity**

Cytotoxic activity against THP-1 and HepG2 cells expressed as IC_{50} and antibacterial activity against *S. aureus*, *E. faecalis*, *E. coli* and *M. catarrhalis* bacteria expressed by MIC were determined for hydrazones **1a-1c**, **2a-2c**, **3a-3c**, **4a-4c** and their parent hydrazides **1-4** (Table 4).

Tested compounds were found noncytotoxic against HepG2 cell line (IC_{50} > 100 μmol/L) but hydrazones showed weak to moderate cytotoxicity on THP-1 cells. Parent hydrazides **1-4** were found noncytotoxic against THP-1. Similar cytotoxicity was previously established for related aroylhydrazones.[43]

Table 4 Cytotoxic and antibacterial activity data for hydrazones and their parent hydrazides.

Compound	IC_{50} (μmol/L)		MIC (μg/mL)			
	THP-1	HepG2	*S. aureus*	*E. faecalis*	*E. coli*	*M. catarrhalis*
1a	17.36	>100	>256	>256	128	16
1b	11.61	>100	>256	>256	128	8
1c	37.81	>100	>256	>256	>256	4
2a	26.81	>100	>256	>256	64	32
2b·H$_2$O	25.33	57.5	>256	>256	64	16
2c·H$_2$O	19.41	>100	>256	>256	128	8
3a	20.61	>100	>256	>256	128	8
3b	17.16	>100	>256	>256	>256	8
3c	15.42	>100	>256	>256	64	8
4a	62.71	>100	>256	>256	>256	16
4b	>100	>100	>256	>256	>256	32
4c	66.51	>100	>256	>256	>256	8
1	>100	>100	>256	>256	>256	256
2	>100	>100	>256	>256	>256	>256
3	>100	>100	>256	>256	>256	256
4	>100	>100	>256	>256	>256	256
Staurosporine	0.33	1.87	–	–	–	–
Azithromycin	–	–	1	2	0.25	0.06

View Article Online
DOI: 10.1039/C7CE02136D

From IC_{50} values of hydrazones obtained on THP-1 cells no trend is observed when either moiety originating from hydrazide or moiety originating from aldehyde is preserved. However, the lowest cytotoxicity was established for hydrazones **4a**-**4c** containing 4-aminobenzhydrazide (**4**).

In general, high minimum inhibitory concentrations (MIC ≥ 128 μg/mL) for all of the investigated compounds indicated no growth inhibition of strains *S. aureus*, *E. faecalis* and *E. coli*. Hydrazides **1**-**4** showed no antibacterial activity on *M. catarrhalis* strain while hydrazones, with their significantly lower MIC values, demonstrated selective activity against *M. catarrhalis* that can be characterized as intermediate. However, the anti-*M. catarrhalis* activity of these compounds is notably lower when compared to reference antibiotic azithromycin. Even though all hydrazones displayed similar MIC values, several observations can be highlighted. When focused on the influence of hydrazide part of hydrazone, hydrazones **1a**, **1b** and **1c** derived from *para*-isomer of pyridine carbohydrazide (**1**) have higher antibacterial activity than corresponding hydrazones **2a**, **2b** and **2c** that contain *meta*-pyridine carbohydrazide (**2**), respectively. In the series of hydrazones containing amino substituted benzhydrazide (**3** or **4**), those with *ortho*-aminobenzhydrazide (**3a** and **3b**) are found to be more active than their respective *para*-isomers (**4a** and **4b**) with the exception of hydrazones **3c** and **4c**. When comparing the effect of aldehyde moiety on activity towards *M. catarrhalis*, the highest activity is exhibited by hydrazones derived from 4-metoxysalicylaldehyde while those from salicylaldehyde showed the lowest activity in the case of **1a**-**1c** and **2a**-**2c** series.

Overall, the results of cytotoxic and antibacterial activity studies suggest that hydrazones **4c** and **1c** are the least cytotoxic and the most potent antibacterial agents making them the most promising compounds for further investigations.

Conclusions

The solution based method results in formation of hydrazones either in the solvent-free form or as solvates or both, depending on the reaction or crystallization conditions. Specific intermolecular interactions between hydrazones or those between hydrazones and solvent molecules are also important in the crystallization processes and determine the structures and compositions of the final products. Eight novel crystal forms are structurally characterized *via* the single crystal X-ray diffraction method revealing the supramolecular assembling role of solvent molecules of crystallization *via* comprehensive analysis of hydrogen bonds patterns in the solid state. This role is the consequence of the proton donor/acceptor competition among functional groups of hydrazones and solvent molecules.

The solid state desolvation route provides an alternative to the conventional method to achieve crystalline unsolvated forms. The mechanochemical strategy employing liquid assisted grinding is demonstrated to be as a successful route for the preparation of the isonicotinic- and nicotinic-based aroylhydrazones. Furthermore, by combining the extensive chemometrical analysis for mechanochemical synthesis monitoring, by using *ex situ* PXRD data with the proper reaction conditions, it is possible to derive a throughout understanding of the reaction processes on molecular level, formation intermediates and reaction periods.

The compounds exhibited no cytotoxic activity on HepG2 and weak to moderate activity on THP-1 cells. No inhibited growth of *S. aureus*, *E. faecalis* and *E. coli* was observed while substantial antibacterial activity was obtained against *M. catarrhalis*.

Experimental section

General remarks

All starting materials and solvents were purchased from commercial sources and used as received without further purification or drying. Elemental analyses were provided by the Analytical Services Laboratory of the Ruđer Bošković Institute, Zagreb. TG analysis was carried out with a Mettler-Toledo TGA/SDTA851e thermobalance using aluminum crucibles. All experiments were recorded in a dynamic atmosphere with a flow rate of 200 cm^3 min^{-1}. Heating rates of 5 K min^{-1} were used for all investigations. DSC measurements were carried out with a Mettler-Toledo DSC823e calorimeter and analyzed by the Mettler STAR^e 9.01. software. FT-IR spectra were recorded on a Perkin Elmer Spectrum Two FTIR Spectrometer using Attenuated Total Reflectance technique (ATR). NMR spectra were recorded on Bruker Avance III HD 400 spectrometer operating at 400 MHz. Compounds were dissolved in DMSO-d_6 and measured in 5 mm NMR tubes at 298 K with TMS as an internal standard. The sample concentration was 10 mg/ml. Electronic absorption spectra of methanol solutions (c = 3× 10^{-5} mol dm^{-3}) were recorded at 25 °C on a Specord 200 UV/Vis (Carl Zeiss, Jena) spectrophotometer with 1 cm quartz cells. Yields and analytical data are given in the Supporting information.

Solution-based synthesis

Hydrazones derived from isonicotinic hydrazide (1a-1c, 1c·H_2O) and nicotinic hydrazide (2a, 2a·H_2O, 2b·H_2O, 2b·MeOH, 2c·H_2O and 2c·MeOH). A mixture of salicylaldehyde, 3-methoxysalicylaldehyde or 4-methoxysalicylaldehyde (5 mmol) and isonicotinic hydrazide or nicotinic hydrazide (5 mmol) in alcohol (methanol or ethanol 250 mL) was refluxed with continuous stirring for 3 h. Unless otherwise stated the obtained solution was cooled and concentrated under vacuum to one third of its volume (see ESI). It was left at room temperature for a few days. The obtained crystalline product was filtered and dried in a dessicator up to constant weight.

Hydrazones derived from 2-aminobenzhydrazide (3a-3c) or 4-aminobenzhydrazide (4a, 4b·MeOH, 4b·EtOH and 4c)

a) Salicylaldehyde dissolved in 40 ml of methanol was added dropwise to a solution of 2-aminobenzhydrazide (5 mmol in 60 mL of methanol) under stirring maintaining the temperature between -5 and 0 °C. After 30 min the mixture was continuously stirred at room temperature for 4 h. The obtained solution was then concentrated under vacuum to one third of its volume. The resulting solution was left at room

View Article Online
DOI: 10.1039/C7CE02136D

temperature for a few days. The obtained crystalline product was filtered and dried in a dessicator up to constant weight.
b) 2-Aminobenzhydrazide or 4-aminobenzhydrazide (5 mmol) was dissolved in 60 mL of alcohol. To this stirred solution was added dropwise a solution of 3-methoxysalicylaldehyde or 4-methoxysalicylaldehyde (5 mmol) in 40 ml of alcohol at 25 °C. After 30 min the mixture was then heated at 40 °C over 4 h under the continuous stirring. Unless otherwise stated the obtained solution was cooled and then concentrated under vacuum to one third of its volume (see ESI). The resulting solution was left at room temperature for a few days. The obtained crystalline product was filtered and dried in a dessicator up to constant weight.

Mechanochemical synthesis

The solid state reactions were carried out using a Retsch MM200 ball mill. Isonicotinic hydrazide (isoniazide), nicotinhydrazide, 2-aminobenzhydrazide or 4-aminobenzhydrazide (1 mmol), and the appropriate aldehyde (1 mmol of salicylaldehyde, 3-methoxy-salicylaldehyde or 4-methoxysalicylaldehyde) and methanol (25 µL) were placed with one 7 mm grinding ball in a 5 mL stainless steel jar.
For the monitoring of the mechanochemical synthesis the reactions were performed each time starting from the reagents and were stopped at the end of the desired reaction time. No purification was performed. Afterwards, samples were analyzed by PXRD and IR spectroscopy. The reactants were ground for 50 min at 25 Hz frequency to obtain **1a**, 70 min at 10 Hz frequency to obtain **1b**, 90 min at 20 Hz frequency to obtain **2a·H$_2$O**, 70 min at 10 Hz frequency to obtain **2b·H$_2$O**, 150 min at 10 Hz frequency to obtain **3b**.

Principal component analysis

Numerical analyses were performed using the second-order tensor decomposition tool principal component analysis, PCA. In PCA, the data matrix with mean-centered columns $\boldsymbol{X}$ of rank r is decomposed as a sum of r matrices $\boldsymbol{t}_i\boldsymbol{p}_i^{\mathrm{T}}$ of rank 1. PCA enables one to find the best linear projections for a high dimensional set of data in the least-squares sense. Scores $\boldsymbol{t}_i$ represent projections of the original sample points on the principal component (PC) direction and can be used for classification or building of probability distributions. Therefore, each point in score plots represents one sample PXRD spectra. Loadings $\boldsymbol{p}_i^{\mathrm{T}}$ represent the eigenvectors of data covariance (or correlation) matrix and can be used for the identification of variability among the data. In this case the physical units of principal components loadings are the same as the intensity units in PXRD spectra. The initial development of PCA goes back to Beltrami[44] and Pearson,[45] whereas the name was introduced by Hotteling.[46] More details on PCA can be found in the literature.[47] Principal component analysis was used as a dimensionality reduction tool and performed using a NIPALS algorithm[48] implemented in our own program ***moonee***.[49,50]

X-Ray crystallography. Powder diffraction.

The powder X-ray diffraction data were collected by the Panalytical X'Change powder diffractometer in the Bragg-Brentano geometry using Cu-K_α radiation. The sample was contained on a Si sample holder. Patterns were collected in the range of $2\theta = 5 - 40°$ with the step size of 0.03° and at 1.5 s per step. The data were collected and visualized using the X'Pert programs Suite.[51] Samples obtained by the mechanochemical synthesis were used immediately for the powder X-ray analysis. Samples of unstable solvates obtained by the solution based method were isolated prior to measurement to avoid loss of solvent as much as possible.

X-Ray crystallography. Single crystal diffraction.

The data collection was carried in the ω scan mode with a Oxford Xcalibur diffractometer equipped with 4-circle kappa geometry and CCD Sapphire 3 detector at different temperatures: 296(2) K for **2b·MeOH**, **2c·MeOH**, **3b**, **4a**, **4b·H$_2$O**, **4c** and at 150(2) K for **4b·MeOH**, **4b·EtOH** and by using graphite monochromated Mo-K_α radiation (λ = 0.71073 Å). Data collection for all structures has been performed by applying the CrysAlis Software system,[52] Version 1.171.37.35. The Lorentz-polarization effect was corrected and the intensity data reduced by the CrysAlis RED.[45]
The diffraction data have been scaled for absorption effects by the multi-scanning method. Structures were solved by direct methods and refined on F^2 by weighted full-matrix least-squares. Programs SHELXT,[53] SHELXL[54] integrated in the WinGX[55] software system (Version 2014.1) were used to solve and refine structures. The C-bound hydrogen atoms were placed in geometrically idealized positions and constrained to ride on their parent atoms, with C–H temperature dependent distances values and with U_{iso}(H) = 1.2U_{eq}(C) or 1.5U_{eq}(C) for methyl H atoms. A rotating model was used for the methyl groups. The hydroxy H atoms of the alcohol molecules and aldehyde part of the ligand molecules were firstly found in a difference Fourier map and then refined by restraining by SHELXL DFIX instruction the O–H bond length to be 0.82 (2) or 0.84 (2) Å, for 296(2) K or 150(2) K data, respectively. The isotropic displacement parameters set to be 1.2 times the equivalent isotropic displacement parameters of the parent oxygen atoms. The analogous refinement procedure has been applied for amine nitrogen and amine atom of amide group (restraints of N–H distance at 0.86(2) Å for 296(2) K and 0.88(2) Å for 150(2) K). The presence of hydrogen atom at amine nitrogen atom of amide group has been additionally confirmed with the metrical parameters of amide group.
The absolute structures have been determined for **3b**, **4a**, **4b·H$_2$O** and **4c** with the corresponding Flack parameters (see Table 4). The molecular geometry calculations were performed by SHELXL[53] and PARST[56] programs. Molecular graphics have been done by program Mercury[57] (Version 3.7).

Table 3 Crystallographic data for compounds **2b·MeOH**, **2c·MeOH, 3b, 4a**, **4b·MeOH**, **4b·EtOH**, **4b·H_2O** and **4c**

Complex	**2b·MeOH**	**2c·MeOH**	**3b**	**4a**	**4b·MeOH**	**4b·EtOH**	**4b·H_2O**	**4c**
Chemical formula	$C_{15}H_{17}N_3O_4$	$C_{15}H_{17}N_3O_4$	$C_{15}H_{17}N_3O_3$	$C_{14}H_{13}N_3O_2$	$C_{16}H_{19}N_3O_4$	$C_{17}H_{21}N_3O_4$	$C_{15}H_{17}N_3O_4$	$C_{15}H_{15}N_3O_3$
M_r	303.32	303.32	285.30	255.27	317.34	331.37	303.32	285.30
Crystal system, habit and colour	Monoclinic, prism, colourless	Monoclinic, prism, colourless	Orthorhombic, prism, colourless	Orthorhombic, prism, colourless	Monoclinic, prism, colourless	Monoclinic, prism, colourless	Orthorhombic Plate, colourless	Monoclinic, prism, colourless
Crystal dimensions / mm^3	0.63 × 0.30 × 0.24	0.42 × 0.23 × 0.11	0.62 × 0.14 × 0.05	0.65 × 0.24 × 0.04	0.20 × 0.18 × 0.04	0.42 × 0.39 × 0.08	0.400.20 0.02	0.59 × 0.38 × 0.12
Space group	$P\,2_1/n$	$P\,2_1/c$	$P\,na2_1$	$P\,na2_1$	$P\,2_1/c$	$P\,2_1/c$	$P\,na2_1$	$P\,c$
Z	4	4	4	4	8	8	4	4
Unit cell parameters:								
a /Å	8.7634(6)	15.6285(5)	9.8994(7)	20.911(2)	18.819(2)	19.2494(10)	24.185(3)	11.9715(5)
b /Å	19.3464(11)	12.4516(4)	6.8199(3)	5.3366(5)	12.3035(8)	12.8121(6)	12.6631(18)	12.5059(6)
c /Å	8.8479(7)	7.3947(3)	20.3396(15)	10.8719(9)	15.245(2)	15.0103(7)	4.7046(8)	9.3710(4)
α/°	90	90	90	90	90	90	90	90
β/°	96.305(7)	93.187(3)	90	90	113.799(16)	112.476(6)	90	97.453(4)
γ/°	90	90	90	90	90	90	90	90
V /Å^3	1491.00(18)	1436.78(9)	1373.19(15)	1213.25(19)	3229.6(7)	3420.7(3)	1440.8 (4)	1391.12(11)
D_{calc} /g cm^{-3}	1.351	1.402	1.380	1.398	1.305	1.287	1.398	1.362
μ /mm^{-1}	0.100	0.104	0.099	0.097	0.095	0.093	0.10	0.097
F(000)	640	640	600	536	1344	1408	640	600
Index range	$h = -10 \to 11$ $k = -21 \to 25$ $l = -11 \to 10$	$h = -17 \to 20$ $k = -13 \to 16$ $l = -7 \to 9$	$h = -13 \to 13$ $k = -9 \to 9$ $l = -17 \to 26$	$h = -27 \to 24$ $k = -7 \to 7$ $l = -14 \to 14$	$h = -24 \to 24$ $k = -15 \to 15$ $l = -19 \to 19$	$h = -19 \to 26$ $k = -17 \to 12$ $l = -20 \to 19$	$h = -32 \to 32$ $k = -16 \to 17$ $l = -6 \to 6$	$h = -13 \to 16$ $k = -17 \to 17$ $l = -12 \to 12$
No. of measured, independent and observed [$I > 2\sigma(I)$] reflections, R_{int}.	4751/ 3114/ 1935, 0.023	6958/ 3460/ 2589, 0.0237	13177/ 2797/ 1834, 0.0625	10403/ 2899/2038, 0.051	31536/7385/5199, 0.0454	18940/9062/5122, 0.038	6479/3564/1467 0.086	15432/6435/3484 0.049
Data / restraints / parameters	3114/3/211	3460/0/ 210	2797/5/202	2899/5/184	5199/10/449	9062/8/467	3564/6/218	6435/9/408
$R[F^2 > 2\sigma(F^2)]$, $wR(F^2)$, S	0.0529, 0.1304, 1.016	0.0449, 0.1148, 1.032	0.0535, 0.1075, 1.06	0.0470, 0.0802, 0.99	0.0488, 0.1034, 1.02	0.0594, 0.1377, 0.98	0.077, 0.109, 0.93	0.0552, 0.097, 0.97
$(\Delta/\sigma)_{max}$	0.004	0.001	0.001	<0.001	<0.001	<0.001	0.001	<0.001
$\Delta\rho_{max}$, $\Delta\rho_{min}$/ e Å^{-3}	0.157, –0.146	0.246, –0.180	0.160, –0.203	0.149, –0.144	0.223, –0.197	0.276, –0.245	0.180, –0.190	0.154, –0.159
Flack parameter	-	-	0.4(10)	–1.4(10)	-	-	–0.4(10)	0.2(9)

View Article Online
DOI: 10.1039/C7CE02136D

Cytotoxicity assay

In vitro cytotoxicity screening of hydrazones **1a-1c**, **2a-2c**, **3a-3c**, **4a-4c** and their parent hydrazides **1-4** was performed on human acute monocytic leukemia (THP-1, ATCC TIB-202) and hepatocellular carcinoma (HepG2, ATCC HB-8065) cells MTS assay was used to ascertain cell viability.[58] HepG2 cells were grown in DMEM/F12 medium while RPMI 1640 medium was used for THP-1. Media were supplemented with 10% heat inactivated fetal bovine serum and 1% antibiotic/antimycotic solution. A total of $5\cdot10^4$ cells were incubated at 37°C in 5% CO_2 atmosphere and 90% relative humidity overnight in microtiter plates with appropriate cell medium containing hydrazone or hydrazide, previously dissolved in DMSO. Hydrazone or hydrazide concentration range of 0.80–100 µmol/L was used in the case of HepG2 and 10^{-4}–100 µmol/L for THP-1. Wells with medium only (blank), wells with cells and medium as well as wells with cells, medium and 1% DMSO served as controls. Wells with cells and staurosporine applied in concentration range 10^{-6}–100 µmol/L served as control of MTS test. After incubation, MTS reagent (CellTiter® Aqueous One Solution Cell Proliferation Assay; Promega) was added to each well and incubation was continued for 1 (Hep-G2) or 6 hours (THP-1). The absorbance of the formed purple formazan was measured at 490 nm using a microplate spectrophotometer Perkin Elmer Victor-2. The average IC_{50} value (the concentration required for 50% decrease in cell viability) was determined from the cell viability *versus* concentration curve with GraphPad Prism software. All experiments were performed in duplicate.

Antibacterial activity assay

Hydrazones **1a-1c**, **2a-2c**, **3a-3c**, **4a-4c** and parent hydrazides **1-4** were tested for their *in vitro* antibacterial activity by the broth microdilution method against two Gram-positive *Staphylococcus aureus* (ATCC 13709) and *Enterococcus faecalis* (ATCC 29212), and two Gram-negative *Escherichia coli* (ECM 1556) and *Moraxella catarrhalis* (ATCC 23246) bacterial strains according to guidelines of the Clinical and Laboratory Standards Institute.[59] *E. coli* strain is hypersensitive due to the efflux pump deficiency (TolC-Tn*10*). *E. faecalis* and *M. catarrhalis* were grown on Columbia agar plates with 5% sheep blood while Mueller-Hinton agar plates were used for *S. aureus* and *E. coli*. After 22 h incubation at 37°C, bacterial inoculum was prepared by direct colony suspension method to a density of 10^8 CFU/mL, which corresponds to a 0.5 McFarland standard. All strains were tested in Mueller-Hinton II Broth (cation-adjusted) culture medium. Tested compound was dissolved in DMSO and applied, in the concentration range 0.5–128 µg/mL, to wells inoculated with bacterial suspension ($5\cdot10^4$ CFU/well). Wells with medium only and wells with medium and bacterial inoculum were also included for sterility and growth control, respectively. For antibacterial susceptibility validation bacteria were also treated with control antibiotic azithromycin (0.03–16 µg/mL). Results expressed as minimum inhibitory concentration (MIC) values were determined by visual inspection after 22 h incubation at 37°C in ambient air. All experiments were performed in duplicate.

Conflicts of interest

There are no conflicts of interest to declare.

Acknowledgments

This work has been fully supported by Croatian Science Foundation under the project (IP-2016-06-4221).

Notes and references

[a] *University of Zagreb, Faculty of Science, Department of Chemistry, Horvatovac, 102a, 10000 Zagreb, Croatia, Fax: ++ 385-1-4606341; Tel: ++385-1-4606353; E-mail: visnja.vrdoljak@chem.pmf.hr*
[b] *University of Zagreb, Faculty of Textile Technology, Division of Applied Chemistry, Prilaz baruna Filipovića 28a, 10000 Zagreb, Croatia*
[c] *University of Zagreb, School of Medicine, Department of Chemistry and Biochemistry, Šalata 3, 10 000 Zagreb*

† Electronic Supplementary Information (ESI) available: (1) schemes of hydrazones, (2) yields and analytical data, (3) PXRD patterns, (3) Chemometric Data Analysis, (4) figures for compounds, (5) tables of selected bond distances and angles and of hydrogen bonds parameters and (7) ^{1}H and ^{13}C NMR spectral data. Crystallographic data sets for the structures **2b·MeOH**, **2c·MeOH**, **3b**, **4a**, **4b·EtOH**, **4b·H_2O**, **4b·MeOH** and **4c** are available through the Cambridge Structural Data base with deposition numbers CCDC 1588275-1588282. See DOI: 10.1039/b000000x/

1 S. L. James, C. J. Adams, C. Bolm, D. Braga, P. Collier, T. Friščić, F. Grepioni, K. D. M. Harris, G. Hyett, W. Jones, A. Krebs, J. Mack, L. Maini, A. G. Orpen, I. P. Parkin, W. C. Shearouse, J. W. Steed, D. C. Waddell, *Chem. Soc. Rev*., 2012, **41**, 413.
2 T. Friščić, *Chem. Soc. Rev*., 2012, **41**, 3493.
3 G.-W. Wang, *Chem. Soc. Rev*., 2013, **42**, 7668.
4 I. Halasz, S. A: J. Kimber, P. J. Beldon, A. M. Belenguer, F. Adams, V. Honkimäki, R. C. Nightingale, R. E. Dinnebier, T. Friščić. T. *Nature Prot*. 2013, **8**, 1718.
5 A. D. Katsenis, A. Puškarić, V. Štrukil, C. Mottillo, P. A. Julien, K. Užarević, M.-H. Pham, T.-O. Do, S. A. J. Kimber, P. Lazić, O. Magdysyuk, R. E. Dinnebier, I. Halasz, T. Friščić, *Nature Commun*. 2015, **6**, 6662.
6 L. Batzdorf, F. Fischer, M. Wilke, K.-J. Wenzel, F. Emmerling, *Angew. Chem. Int. Ed*. 2015, **54**, 1799.
7 K. Užarević, I. Halasz, T. Friščić, J. *Phys. Chem. Lett*. 2015, **6**, 4129.
8 I. Halasz, T. Friščić, S. A. J. Kimber, K. Užarević, A. Puškarić, C. Mottillo, P. Julien, V. Strukil, V. Honkimaki and R. E. Dinnebierd, *Faraday Discuss*., 2014, **170**, 203.
9 D. Braga, S. L. Giaffreda, F. Grepioni, M. Polito, *CrystEngComm*, 2004, **6**, 458.
10 G. A. Bowmaker, Effendy, J. V. Hanna, P. C. Healy, S. P. King, C. Pettinari, B. W. Skelton, A. H. White, *Dalton Trans*., 2011, **40**, 7210.
11 D. Tan, L. Loots, T. Friščić, *Chem. Comm*, 2016 , **52**, 7760.
12 N. Belkheri, D. Bougerne, F. Bedos-Beval, H. Duran, C. Bernis, R. Salvayre, A. Négre-Salvayre, M. Baltas, *Eur. J. Med. Chem*., 2010, **45**, 3019.
13 G. Verma, A. Marella, M. Shaquiquzzaman, M. Akhtar, M. R. Ali, M. M. Alam, *J Pharm. Bioall. Sci.* 2014, **6**, 69.
14 S. Rollas, Ş. Güniz Küçükgüzel, *Molecules* **2007**, 12, 1910.
15 R. Dabideen, K. F. Cheng, B. Aljabari, E. J. Miller, V. A. Pavlov, Y. Al-Abed, *J. Med. Chem*., 2007, **50**, 1993.
16 G. Kaupp, J. Schmeyers, J. Boy, *J. Prakt. Chem*., 2000, **342**, 269.
17 G. Kaupp, J. Schmeyers, *J. Phys. Org. Chem*., 2000, **13**, 388.
18 P. F. M. Oliviera, M. Baron, A. Chamayou, C. André-Barrès, B. Giidetti, M. Baltas, *RSC Advances*, 2014, **4**, 56736.
19 V. Vrdoljak, G. Pavlović, T. Hrenar, M. Rubčić, P. Siega, R. Dreos, M. Cindrić, *RSC Advances* 2015, **5**, 104870.
20 V. Vrdoljak, B. Prugovečki, D. Matković-Čalogović, J. Pisk, R. Dreos and P. Siega, *Cryst. Growth Des*., 2011, **11**, 1244.

View Article Online
DOI: 10.1039/C7CE02136D

21 V. Vrdoljak, B. Prugovečki, D. Matković-Čalogović, T. Hrenar, R. Dreos and P. Siega, *Cryst. Growth Des*., 2013, **13**, 3773.
22 A. Nangia, G. R. Desiraju, *Chem. Commun*., 1999, 605.
23 C. Bilton, J. A. K. Howard, N. N. L. Madhavi, A. Nangia, G. R. Desiraju, F. H. Allenc, C. C. Wilson, Chem. Comm., 1999, 1675.
24 T. Sakai, K. Katagiri, Y. Uemura, H. Masu, M. Tominaga,I. Azumaya, *Cryst. Growth Des*. 2013, **13**, 308.
25 V. S. Sergienko, V. L. Abramenko, L. Kh, M. A. Porai-Koshits, V. G. Sahkarova, *Koord. Khim. Russ. Coord. Chem*., 1993, **19**, 28.
26 B. Liu, R.-X. Hu, Z.-F. Chen, X.-B. Chen, H. Liang, K.-B. Yu, *Chin. J. Struct. Chem*., 2002, **21**, 414.
27 H. D. Yin, M. Hong, G. Li, D. Q. Wang, *J. Organomet. Chem*., 2005, **690**, 3714.
28 Y.-J. Xu, S. Zhao, S. Bi, *Acta Crystallogr. Sect. E*, 2007, **63**, o4633.
29 M. Yu, X. Chen, Z.-L. Jing, *Acta Crystallogr. Sect. E*, 2005, **61**, o1345.
30 D.-S. Yang, *J. Chem. Cryst*. , 2007, **37**, 343.
31 J. Xu, Synth. React. Inorg. , *Met.-Org., nano-Met. Chem*., 2013, **43**, 1329.
32 M. R. J. Elsegood, M. Kose, E. Akgun, *CSD Communication*, 2015
33 F. Zhi, R. Wang, *Acta Crystallogr. Sect. E*, 2010, **66**, o892.
34 S.-J. Peng, H.-Y. Hou, *Acta Crystallogr. Sect. E*, 2008, **64**, o1996.
35 N. Galić, B. Perić, B. Kojić-Prodić, Z. Cimerman, *J. Mol. Struct*., 201, **559**, 187.
36 N. Mathew, M. Kuriakose, E. B. Seena, M. R. P. Kurup, *Acta Crystallogr. Sect. E*, 2007, **63**, o2190.
37 R. Dinda, P. Sengupta, S. Ghosh, H. Mayer-Figge, W. S. Sheldrick, *J. Chem. Soc., Dalton Trans*., 2002, 4434.
38 B. Levrand, Y. Ruff, J. -M. Lehn and A. Herrmann, *Chem Comm*. 2006, 2965-2967.
39 R. Nguyen, I. Huc, *Chem. Commun*, 2003, 942.
40 P. Ramadevi, R. Singh, A. Prajapati, S. Gupta, D. Chakraborty, Hindawi Publishing Corporation Advances in Chemistry Volume 2014, Article ID 630575, 14 pages http://dx.doi.org/10.1155/2014/630575
41 S. Çakıra, E. Biçer, *J. Iran. Chem. Soc*., 2010, **7**, 394.
42 S. P. Sovilj, V. M. Vasi, D. L. Stoji, B. Stojeva-Radovanovi, L. T. Petkovska, *Spectros. Lett*., 1998, **31**, 1107.
43 M. Cindrić, A. Bjelopetrović, G. Pavlović, V. Damjanović, J. Lovrić, D. Matković-Čalogović, V. Vrdoljak, *New J. Chem.* 2017, **41**, 2425.
44 E. Beltrami, *Giornale di Matematiche ad Uso degli Studenti Delle Universita*, 1873, **11**, 98.
45 K. Pearson, *Philos. Mag.*, 1901, **2**, 559.
46 H. Hotelling, *J. Educ. Psychol.*, 1933, **24**, 417.
47 I. T. Jolliffe, *Principal Component Analysis*, Springer, Berlin, 1986.
48 P. Geladi, B. Kowalski, *Anal. Chim. Acta* 1986, **185**, 1.
49 T. Hrenar, ***moonee***, Program for Manipulation and Analysis of Multi- and Univariate Data, rev. 0.6827, 2017.
50 O. Jović, T. Smolić, I. Primožič and T. Hrenar, *Anal. Chem.* 2016, **88**, 4516.
51 *X'Pert Software Suite*, Version 1.3e; Panalytical B. V., Almelo, The Netherlands, 2001.
52 CrysAlisPro, Agilent Technologies, Version 1.171.37.35.
53 G. M. Sheldrick, Acta Crystallogr. 2015, C71, 3.
54 G. M. Sheldrick, Acta Crystallogr. 2015, A71, 3.
55 L. J. Farrugia, J. Appl. Crystallogr., 2012, 45, 849.
56 (a) M. Nardelli, Comput. Chem. 1983, 7, 95; (b) M. Nardelli, J. Appl. Cryst. 1995, 28, 659.
57 C. F. Macrae, I. J. Bruno, J. A. Chisholm, P. R. Edgington, P. McCabe, E. Pidcock, L. Rodriguez-Monge, R. Taylor, M. Towler, J. Van der Streek and P. A. Wood, J. Appl. Crystallogr. 2008, 41, 466.
58 T. Mosmann, *J. Immunol. Methods*, 1983, **65**, 55.
59 CLSI. Methods for Dilution Antimicrobial Susceptibility Tests for Bacteria that Grow Aerobically; Approved Standard-Eight edition. CLSI document M07-A8. Wayne, PA: Clinical and Laboratory Standards Institute; 2009.

View Article Online
DOI: 10.1039/C7CE02136D

Table of contents entry

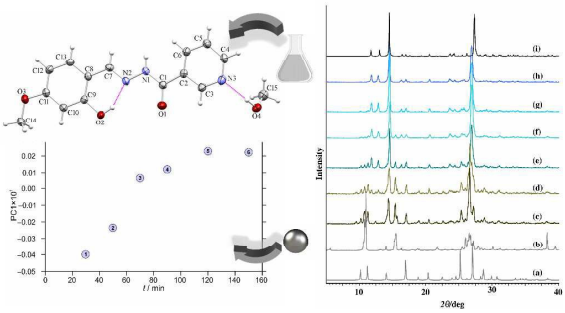

In this manuscript we describe for the first time the implementation of chemometric analysis for the mechanochemical synthesis monitoring.